








Cite this: *Phys. Chem. Chem. Phys.*,
2023, 25, 1269

Dielectric switching in correlation with the structural phase transitions in tetrapropylammonium perchlorate†

Monika Trzebiatowska, ^a Dorota A. Kowalska, ^a Marek A. Gusowski, ^{*b}
Ewelina Jach ^b and Agnieszka Cizman ^b

The crystals of the tetrapropylammonium perchlorate ($[(CH_3CH_2CH_2)_4N]ClO_4$, TePrAClO₄) compound undergo two reversible phase transitions: at ca. $T_1 = 284$ K and at ca. $T_2 = 445$ K. The observed phase transitions and distinct dielectric and relaxation effects are due to the dynamic motions of the organic cations and anionic framework. The crystals become ordered at low temperatures, then disordered at room temperature (propyl chains of the organic part as well as perchlorate ions are disordered over the mirror plane at $c = 1/4$ and $3/4$) and highly disordered at high temperatures. The comparable changes in the wavenumber and FWHM shifts (IR and Raman spectroscopy) in the case of tetrapropylammonium and perchlorate ions in the phase transition at T_1 and slightly more significant changes for organic cations (juxtaposed with perchlorate ions) in the phase transition at T_2 lead to a conclusion that the phase transition at T_1 is equally driven by motions of the two ions, while the phase transition at T_2 is more influenced by the motions of organic cations. The phase transition at T_2 with its large entropy change resembles the behavior found in liquid crystals. The dielectric function values can be switched and tuned in the low- and high-dielectric states, which may indicate the potential application of this material in sensors or actuators.

Received 9th August 2022,
Accepted 30th November 2022

DOI: 10.1039/d2cp03665g

rsc.li/pccp

Introduction

Some compounds may hide some of their properties for a very long time before being rediscovered. In particular, the family of perchlorate salts with simple amines is underrated in this regard. However, their great come back has been noticed as they often show ferroelectric or ferroelastic properties combined with the presence of phase transitions. A remarkable example of this return is the case of a complex of tetraethylammonium perchlorate (abbreviated hereafter as TeECIO₄). This crystal was first discovered in the 1990s^{1,2} and it took over ten years to discover it as a molecular ferroelectric.³ It has been found that this crystal is ferroelectric at room temperature (RT), with a very high polarization value, and it undergoes a phase transition (PT) at 360/380 K (cooling/heating) from the polar monoclinic *Cc* to (most probably) the nonpolar cubic *Fm* $\bar{3}$ *m*

space group. This PT is followed by a sudden change in the values of the dielectric function. It has been concluded that the ferroelectric properties of the low-temperature (LT) phase originate from the relative displacement of cations (tetraethylammonium) and anions (perchlorate) in the same layer and that the material possesses a high number of crystallographically equivalent polarization directions, equal to 24.

Other examples of perchlorates complexed with ammonium molecules include their complexes with guanidinium (Gua)^{4,5} several N-heterocyclic ammonium cations such as piperazinium (Pipa),⁶ and derivatives of piperidinium (Pipd),⁷ 1,4-diazabicyclo[2.2.2]octane (Dabco),⁸ and imidazolium (Im).⁹ These materials mostly possess a perovskite-like structure with incorporated potassium ions, wherein the perchlorate anions along with K⁺ create a 3D framework with voids complemented by the protonated ammonium cations. They all experience a phase transition at a certain temperature, covering the range of 300–450 K. An extreme case of multiple PTs is observed in PipaKClO₄ with three subsequent phase transitions, going from *Pbca* through *Pbcm* with an increasing disorder of both H₂Pipa²⁺ and ClO₄[−] ions and with an increase in temperature. Some crystals exhibit additional extraordinary features, such as an electromechanical coupling found in ImKClO₄ with a piezo-response exceeding by 150% that of the well-known lead

^a Institute of Low Temperature and Structure Research, Polish Academy of Sciences, 50-422 Wrocław, Poland

^b Faculty of Fundamental Problems of Technology, Wrocław University of Science and Technology, Wybrzeże Wyspiańskiego 27, 50-370, Wrocław, Poland.
E-mail: marek.gusowski@pwr.edu.pl

† Electronic supplementary information (ESI) available. CCDC 2195872. For ESI and crystallographic data in CIF or other electronic format see DOI: <https://doi.org/10.1039/d2cp03665g>



zirconate titanate (PZT) ceramics and almost 300% that of the VDF-TrFE polymer.⁹

All perchlorate complexes have been proved to be stable up to a very high temperature of 500 K and even beyond which makes them good candidates for different applications, such as thermal imaging, mechanical actuation or data storage.¹⁰

Attracted by the numerous interesting features of perchlorates, such as ferroelectricity, piezoelectricity, and dielectric switching as well as their interesting and sometimes unexpected phase transitions, we have decided to search for other perchlorate-based materials. It has been shown, in the case of the long-known material: tetrapropylammonium perchlorate, $[(\text{CH}_3\text{CH}_2\text{CH}_2)_4\text{N}]\text{ClO}_4$, that new surprising features may appear. The study of this materials has been so far only limited to a low-temperature (LT) crystal structure.¹¹ No other results have been found regarding this, as we will show, fascinating material.

Experimental

Synthesis

All reagents (analytical grade) used for the synthesis were commercially purchased from Sigma-Aldrich and used without further purification. In order to obtain $(\text{CH}_3\text{CH}_2\text{CH}_2)_4\text{N}\cdot\text{ClO}_4$, 5 mmol of $(\text{CH}_3\text{CH}_2\text{CH}_2)_4\text{NCl}$ and 5 mmol of HClO_4 were dissolved in 20 ml of methanol. The solution was allowed to stand at room temperature. The crystals were harvested after two days. The corresponding PXRD diagrams at different temperatures are presented in Fig. S1 in the ESI†

Structure analysis

The single-crystal X-ray diffraction patterns were collected on an Oxford X'Calibur four-circle diffractometer operating with

graphite-monochromated $\text{MoK}\alpha$ radiation ($\lambda = 0.71073 \text{ \AA}$). The Oxford open-flow heating-cooling system maintained nonambient temperatures. For data processing, CrysAlis PRO¹² and CrysAlis RED¹³ software programs were used. The crystal structures were solved by direct methods and refined using the SHELX crystallographic software package.¹⁴ Olex2¹⁵ software was used to prepare data for publication. Diamond¹⁶ software was used to create graphical representations of the crystal structure. The crystallographic details concerning the crystal, data collection and refinement details are presented in Table 1 and Table S1 (ESI†).

All non-hydrogen atoms were refined anisotropically. The positions of the H atoms from TePrA^+ moieties were refined with fixed C—H distances using HFIX 23 and HFIX 137 (for terminal carbon atoms) instructions. The attempts to collect single-crystal X-ray diffraction data for TePrAClO_4 after the second phase transition (PT2) at 445 K were unsuccessful. The single-crystal cracking was observed and then the conversion into powder occurred. For the completion of crystal characterization, the high temperature powder X-ray diffraction (PXRD) studies were performed on a PANalytical X'Pert diffractometer equipped with a PIXcel solid-state linear detector. For the sample heating/cooling from RT to 478 K an Anton Paar high-temperature attachment was utilized. $\text{CuK}\alpha$ radiation ($\lambda = 1.5418 \text{ \AA}$), generated at 40 kV and 30 mA, in reflection mode was used for registering X-ray diffraction patterns. Data treatment was carried out using PANalytical X'Pert HighScore Plus software.

IR and Raman spectroscopy

The temperature-dependent infrared spectra were measured in a heating mode on KBr pellets in the range $4000\text{--}550 \text{ cm}^{-1}$ using a Nicolet iN10 Fourier transform IR spectrometer

Table 1 Diffraction experimental details for LT and RT phases. For all phases: $M_r = 285.80$, $Z = 4$; chemical formula: $(\text{C}_3\text{H}_7)_4\text{N}\cdot\text{ClO}_4$; crystal form: block; crystal colour: colourless; crystal size: $0.54 \times 0.22 \times 0.17 \text{ mm}$; numerical absorption correction based on Gaussian integration over a multifaceted crystal model was applied

Phase	LT ^a	RT
Crystal data		
Crystal system	Orthorhombic	Orthorhombic
Space group	$P2_12_12_1$ (no. 19)	$Pnma$ (no. 62) ^b
Temperature (K)	100	295
a, b, c (Å)	13.215(3), 12.106(3), 9.641(2)	13.655(4), 12.257(4), 9.758(3)
V (Å ³)	1542.4(6)	1634.4(9)
μ (mm ⁻¹)	0.26	0.24
Data collection		
Refl. measured/unique/observed [$I > 2\sigma(I)$]	43 339/3943/3795	40 477/1767/1409
R_{int}	0.023	0.030
$(\sin \theta/\lambda)_{\text{max}}$ (Å ⁻¹)	0.676	0.625
Refinement		
$R[F^2 > 2\sigma(F^2)], wR(F^2), S$	0.024, 0.063, 1.08	0.038, 0.111, 1.05
Data/parameters/restraints	3943/169/0	1767/171/0
Extinction coefficient	0.0051(10)	0.0059(11)
$\Delta\rho_{\text{max}}, \Delta\rho_{\text{min}}$ (e Å ⁻³)	0.23, -0.33	0.18, -0.23
Absolute structure	Refined as an inversion twin	—
Abs. struct. param.	0.42(5)	—

^a Data can be compared with those previously measured by Fujihara *et al.*¹¹ at 173 K. ^b The non-standard setting of the space group $Pnma$ was chosen for comparison with the LT phase.



equipped with a ZnSe-Linkam cryostat cell THMS600 with a temperature stability of 0.1 K, a liquid nitrogen (LN2) cooled mercury-cadmium-telluride detector, a permanently aligned $15\times$ objective, a 0.7 numerical aperture with a working distance set at 16 mm.

The Raman spectra were measured in heating mode using a Renishaw InVia Raman spectrometer equipped with a confocal DM 2500 Leica optical microscope, a thermoelectrically cooled CCD as a detector, and an Ar^+ laser operating at 488 nm. The spectral resolution in IR and Raman experiments was set at 2 cm^{-1} . Due to the sublimation of the sample and its subsequent deposition on a measurement window, which blocked the laser beam, we had to stop the experiment at 470 K, just before the second PT, although the onset of the second PT can be still observed as the laser heat led to additional heating of the sample.

DSC measurements

Differential scanning calorimetry (DSC) measurements, over the temperature range 200–450 K with a heating rate of 10 K min^{-1} , were performed using a Mettler Toledo DSC-1 instrument. The measurements were carried out by heating and cooling the polycrystalline samples in aluminum crucibles under a nitrogen atmosphere at atmospheric pressure.

Dielectric measurements

The complex dielectric permittivity ε ($\varepsilon = \varepsilon' - i\varepsilon''$) of TePrAClO_4 compounds was measured using the Dynamic Impedance Spectroscopy (DIS) method on a Novocontrol Alpha Analyzer in a frequency range 10 Hz–1 MHz and in the temperature range from 200 K to 450 K. The powder-pressed pellet plates deposited with silver conducting paste were used and the measuring AC voltage was 1 V.

Results and discussion

Thermal properties

In order to detect heat anomalies during the cooling and heating processes related to the phase transition triggered by temperature, the DSC method has been used. The DSC scans of TePrAClO_4 reveal two reversible heat anomalies at around 284 K and 445 K (Fig. 1).

The PT observed at 284 K (PT1) plotted in Fig. 1 can be regarded rather as a continuous phase transition due to the quasi-continuous character of entropy changes, approaching $10\text{ J mol}^{-1}\text{ K}^{-1}$, which puts the title crystal in the same row as other perchlorate perovskites, such as dabco- KClO_4 or piperazinium- NaClO_4 .⁸ Using the Boltzmann equation, the number of disordered sites in the RT phase is calculated to be 2.8, suggesting a disorder in this phase.

Sharp anomalous peaks at 432 K upon cooling and at 449 K upon heating (PT2) together with a large hysteresis of about 17 K and step-like changes of entropy around the phase transition temperature (Fig. 2) suggest a discontinuous first-order character of the PT of the TePrAClO_4 compound at T_2 .

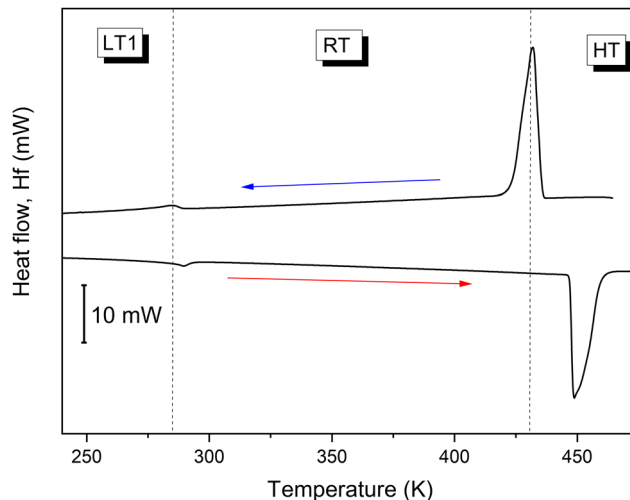


Fig. 1 The DSC curve of the TePrAClO_4 compound.

Moreover, a large entropy change associated with the PT, reaching $130\text{ J mol}^{-1}\text{ K}^{-1}$, suggests a great number of degrees of freedom and a giant disorder in the HT phase, where both TePr^+ and ClO_4^- ions could become disordered. The entropy value is still much higher here than those reported for trimethylethylammonium- ClO_4 , which is around $40\text{ J mol}^{-1}\text{ K}^{-1}$.¹⁷ Actually, it is close to the values obtained for phase changes in liquid crystals, which may go up to several hundreds of $\text{J mol}^{-1}\text{ K}^{-1}$.¹⁸ There is a clear dependence of the ΔS on the composition of the molecules constituting liquid crystals. For example, each methyl or methylene unit (here contained in the four propyl chains in TePr^+ cation) contributes around 18 and $7\text{ J mol}^{-1}\text{ K}^{-1}$, respectively, to the overall ΔS in the phase change from the crystal at RT to the isotropic liquid at HT.^{18,19} Therefore, we might suspect that a similar transition takes place at HT in the title crystal, resulting in an

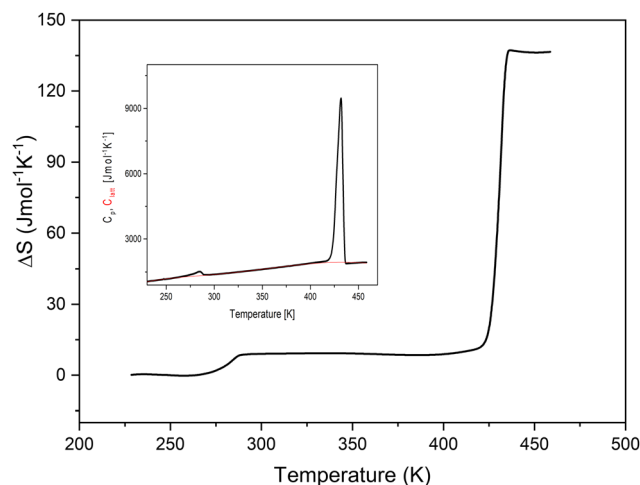


Fig. 2 The temperature dependence of entropy changes of TePrAClO_4 . The inset shows the measured specific heat (C_p) and calculated lattice heat (C_{latt}).



extremely disordered crystal resembling a quasi-isotropic liquid.

Structural data

The X-ray diffraction studies have shown that TePrAClO_4 crystallizes at RT in the orthorhombic system with the $Pnam$ symmetry (RT phase), which is characterized by a disorder of propyl chains and perchlorate anions. Upon cooling, the structure undergoes a reversible phase transition (PT1) to the ordered orthorhombic LT phase with the $P2_12_12_1$ symmetry (Fig. 3) at $T_1 = 284$ K. Due to the symmetry reduction at the PT point, the sample becomes twinned.

In the HT phase, the quality of the crystal was insufficient for single-crystal X-ray diffraction analysis, so the second reversible phase transition (PT2), at $T_2 = 445$ K, to the HT phase was confirmed by powder X-ray diffraction (Fig. S1, ESI[†]). The comparison of the PXRD pattern of the RT phase with the simulated one based on the crystal data proves good purity of the measured sample (shown in the inset of Fig. 4). A reduction in the number of diffraction peaks in the PXRD diagrams is observed (e.g. the diffraction peaks at 11.8, 16, 18.4, 20.8, 24.4, 26.1, and 27.9° disappeared) as the temperature increases, thus we suspect that the change leads to a highly symmetric structure, although we are not able to provide a more accurate description. The structure of the HT phase cannot be indexed unambiguously even if based on the known RT phase. The attempts made to solve the structure of the HT phase failed, presumably due to the lack of a simple transformation between the unit cell of RT and HT phases as well as a magnifying inherent disorder. It must be noted that the poor quality and highly disordered crystals in the HT phase can be regarded as characteristic features for organic-inorganic hybrid compounds with perchlorate anions, such as TeECLO_4^3 or with chloromethyl-triethylammonium cations' RT phase.²⁰

The asymmetric unit comprises two disordered ions: TePrA^+ with C and H atoms disordered over a mirror plane perpendicular to the c -axis direction and ClO_4^- with disordered O atoms (Fig. S2b and S3b, ESI[†]). Due to the presence of disorder, the perchlorate ions are strongly distorted, the six tetrahedral angles are ranging from 93.4(6)–127.4(9)°. The TePrA^+ ions are aligned in layers in the structure (Fig. 5b). The perchlorate ions are located among them creating together a net of hydrogen bonds (HBs) that stabilize the structure (Fig. 5d and

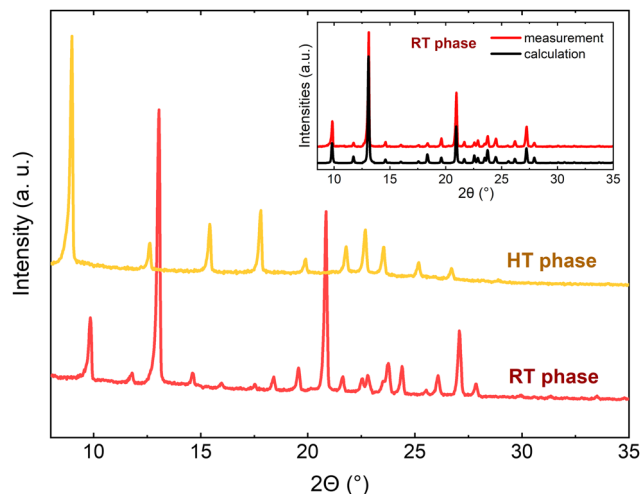


Fig. 4 The PXRD diagrams for the RT and HT phases of TePrAClO_4 showing the reduction of crystal symmetry upon heating the sample. The comparison of the PXRD pattern of the RT phase to the simulated based on the crystal data is shown in the inset.

Table S2, ESI[†]). Each of the ClO_4^- ions is surrounded by four TePrA^+ cations and also every cation has four perchlorate anions as neighbours.

LT phase. The composition of the asymmetric unit in the LT phase remains the same as in the RT phase (Fig. 3a and Fig. S2a, ESI[†]). The structure changes symmetry to the lower symmetry space group $P2_12_12_1$.¹¹ Although the LT phase has been determined at 100 K, the structure agrees with the one previously published by Fujihara *et al.*,¹¹ measured at 173 K (to make the comparison easier, all atoms in the presented structures have been named in the same manner as in ref. 11). However, due to the temperature lowering, some differences can be found, e.g. the distortions of ClO_4^- tetrahedra are less noticeable (at 100 K, the O—Cl—O angles are close to ideal tetrahedral angles [108.78(7)–109.95(9)°], and at 173 K, they range from 106.78(4)–111.13(14)°¹¹), the bond lengths have a smaller range at lower temperature (Cl—O bonds: 1.435(2)–1.443(2) Å vs. 1.384(2)–1.414(2) Å, at 100 K and 173 K, respectively; C—N bonds: 1.523(2)–1.528(2) Å vs. 1.508(3)–1.531(3) Å, at 100 K and 173 K,¹¹ respectively). As one could expect, all of

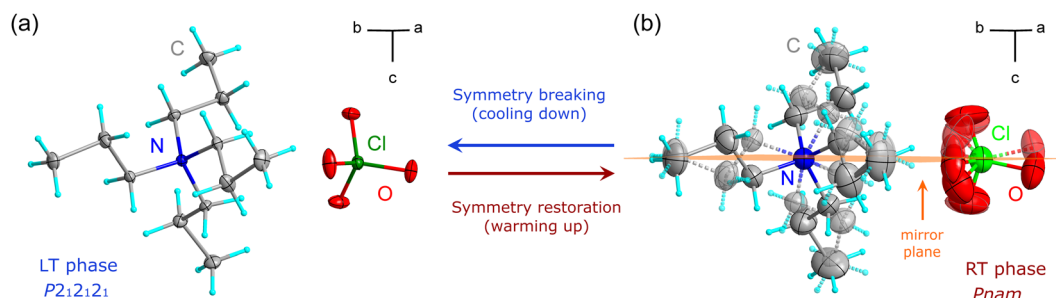


Fig. 3 The symmetry change in TePrAClO_4 as the temperature increases from (a) the LT phase to (b) the RT phase.



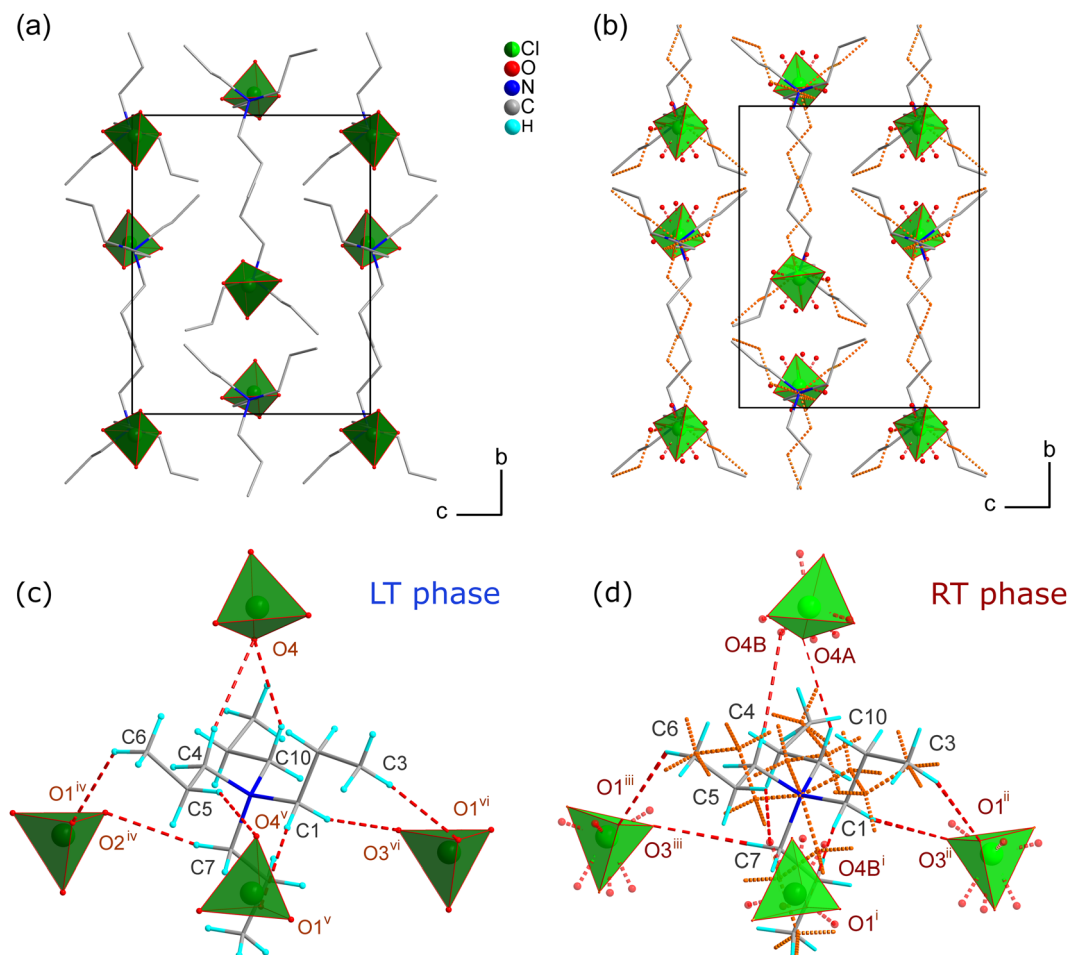


Fig. 5 The view of the crystal structure in the LT phase at 100 K (a) compared to the corresponding view in the RT phase at 295 K (b). The hydrogen atoms and HBs are removed for presentation clarity. Red dashed lines in (c and d) designate C—H...O hydrogen bonds. HBs from the disordered parts (d) are omitted for the sake of clarity. (b and d) The disordered TePrA⁺ cations over *m* planes are marked with orange dashed lines. Disordered oxygen atoms from perchlorate anions are presented with a transparency of 0.35. Symmetry codes: (i) $x - 1/2, -y + 3/2, z$; (ii) $-x + 1/2, y + 1/2, -z$; (iii) $-x + 1/2, y + 1/2, z + 1/2$; (iv) $-x + 1, y + 1/2, -z + 1/2$; (v) $x - 1/2, -y + 3/2, -z$; (vi) $-x + 1, y + 1/2, -z - 1/2$.

HBs, which remain in the structure, are shorter after PT1 (see Table S2, ESI[†]). At 100 K, the structure is completely ordered. However, additional XRD measurements above and below PT1 have been made to confirm the structural phase transition at this temperature (see sections of reciprocal space presented in Fig. S3, ESI[†]). The experiment made *ca.* 10 K below the phase transition, *i.e.* at 275 K (for the diffraction experiment detail see Table 1 and Table S1, ESI[†]), let us observe that not all of the TePrA⁺ cations are ordered. The amount of disordered TePrA⁺ was refined to be 11%. Also, the perchlorate ion is not completely ordered at this temperature. Two of its oxygen atoms (O2 and O4) are disordered over two positions (Fig. S4, ESI[†]).

IR and Raman spectroscopy

The observed IR and Raman modes along with their assignment are given in Table S3 (ESI[†]). The factor group analysis has been omitted due to the fact that both tetrapropylammonium (TePrA⁺) cations and perchlorate anions are disordered at higher temperatures. The temperature-dependent IR spectra in full range and their details are

presented in Fig. S5 and S6 (ESI[†]), respectively, while the Raman spectra are shown in Fig. S7 and S8 (ESI[†]), respectively. We have plotted the relations of some selected bands' position and their corresponding full widths at half maximum (FWHMs) as the function of temperature in Fig. S9 (IR) and S10 (Raman) (ESI[†]).

Basically, the observed bands originate from internal vibrations of TePrA⁺ cations and perchlorate anions as well as their translations and hindered rotations. The two phase transitions are clearly visible in both IR and Raman spectra, even though the Raman experiment had to be stopped in the middle of the PT2 due to the reasons explained in the Experimental section. The spectra show that PT1 should rather be regarded as first-order, while PT2 is abrupt and thus definitely of first order. Additionally, PT2 occurs with much larger thermal effect (based on the FWHMs changes) compared to PT1.

Since the literature for the assignment of vibrations of both ClO₄[−] and TePrA⁺ ions is quite rich,^{21–28} we will further focus on two features: (i) the real symmetry of the crystal and (ii) the influence of temperature on its behavior near PTs.



Normally, an unperturbed tetrahedral ClO_4^- anion has nine normal modes. Its vibrational representation under the T_d point group is: $A_1 + E + 2F_2$, leading to four vibration frequencies groups (in wavenumbers): symmetric stretching $\nu_s\text{ClO}_4^-$ (A_1) at ca. 930 cm^{-1} , symmetric bending $\delta_s\text{ClO}_4^-$ (E) at ca. 460 cm^{-1} , asymmetric stretching $\nu_{as}\text{ClO}_4^-$ (F_2) at ca. 1100 cm^{-1} and asymmetric bending $\delta_{as}\text{ClO}_4^-$ (F_2) at ca. 620 cm^{-1} . All of them are Raman active, but only two of them, of F_2 symmetry, are also infrared active.^{23,29} However, due to the placement in a crystal, with the imposed site and factor-group symmetry, the bands should be split into several more. The main difference between the two phases (LT and RT) is the absence/presence of an inversion center, which means that in the LT phase, some modes are both IR- and Raman-active, while in the RT phase, they should be either IR- or Raman active (mutual exclusion rule). For example, when the anion is placed in C_1 site symmetry and factor group D_2 (LT-phase = $P2_12_12_1$), the A_1 mode should be composed of one Raman-active A mode and three IR- and Raman active B_1 , B_2 and B_3 modes; while in C_s site symmetry with imposed factor group D_{2h} (in RT phase = $Pnam$), A_1 will transform into Raman-active: A_g , B_{3g} and IR-active B_{1u} , B_{2u} . Therefore, for this particular mode, we should observe 4 (2) Raman and 3 (2) bands in the LT (RT) phase. In reality, there are 2 (1) Raman and 2 (1) IR modes visible in the LT (RT) phases, respectively. The lesser number of modes may be caused by a very weak absorption/intensity of a given band, a superposition of the bands and a real symmetry being different from expected as well as quite weak intermolecular interactions. The latter two facts are deduced. First, the center of symmetry is manifested in the simplest scenario by the fact that IR-active modes should be absent in the Raman spectra and *vice versa*. Here, this should apply to the RT phase; however, the observations prove different: the counterparts are observed both in IR and Raman spectra (though usually not with the same absorption/intensity). This leads to a conclusion that despite an apparent centrosymmetric arrangement, the real symmetry of the crystal is distorted resulting in the persistent absence of the center of symmetry, at least to a certain extent. Second, the splitting of totally symmetric A_1 mode may result only from the factor group splitting. Thus, the rather weak intermolecular interactions are confirmed here as the A_1 mode is split into a lesser number of modes than expected from the group theory. In general, the number of modes for ClO_4^- anions is smaller than anticipated except for the $\nu_{as}\text{ClO}_4^-$ (F_2) mode with the center at ca. 1100 cm^{-1} . This band consists of multiple superimposed bands that originate from mutual interactions of the modes within one anion.

The case of TePrA^+ cations is much more complicated than that of ClO_4^- anions in terms of symmetry considerations because one should examine every propyl chain separately (due to some differences in the bond lengths and angles) and it is practically impossible given the disorder at higher temperatures. Therefore, we will discuss its vibrations only with respect to its thermal features.

The disorder at higher temperatures is clearly seen in both IR and Raman spectra including the vibrations of both organic

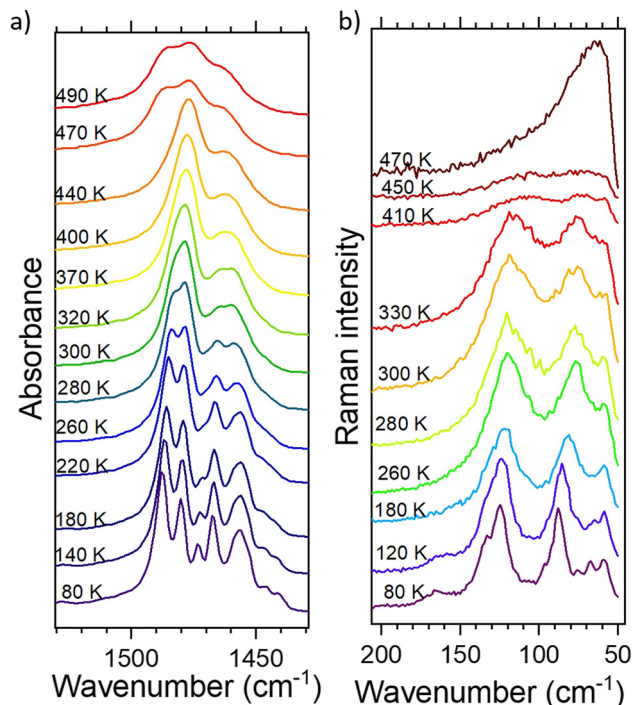


Fig. 6 The thermal evolution of: (a) deformation CH_3 and CH_2 vibrations (IR) and (b) translations and librations of ClO_4^- and TePrA^+ ions.

and inorganic ions (see Fig. 6 and Fig. S6, S8, ESI†). In Fig. S9 and S10 (ESI†), we have presented the values of wavenumber and FWHM of some selected bands, which showed the most remarkable changes upon the PTs. Basically, all the bands broaden and shift with temperature increase. There are two sudden changes during the cooling/heating corresponding to both PTs observed in DSC. The temperatures obtained by IR/Raman spectroscopy agree with the ones from DSC quite well. In the figures cited above, one can see that PT1 (LT-to-RT transition) is less pronounced than PT2 (RT-to-HT), though still clearly noticeable.

The changes regarding ClO_4^- anion include wavenumber shifts towards lower values by $<1\text{ cm}^{-1}$ for PT1 and a few cm^{-1} during PT2 for $\nu_s\text{ClO}_4^-$, $\delta_{as}\text{ClO}_4^-$ and librations of this anion, while its translations move drastically from over 120 cm^{-1} down to almost 60 cm^{-1} in PT2 (depicted in Fig. S9 (IR) and S10 (Raman), ESI†). The FWHM values approach $1\text{--}3\text{ cm}^{-1}$ in PT1 and up to 17 cm^{-1} in PT2 (although Raman spectra did not go beyond the PT2 point due to the difficulties described in the Experimental section). They are comparable with those obtained for inorganic perchlorates, like e.g. KClO_4 .²⁶ The band corresponding to $\nu_s\text{ClO}_4^-$ (Fig. S6, ESI†) in IR spectra does not change the center of gravity but one can notice that it loses its features as the temperature increases and becomes much broader at the final temperature. This clearly proves the onset of the disorder in the perchlorate tetrahedral, specifically taking into account its libration dynamics so well presented in Fig. 6b, leading to a conclusion that the anions are set free above 470 K .



The thermal changes inside the TePrA^+ cations encompass both the modes of CH_3 and CH_2 moieties as well as skeleton vibrations. This disorder is particularly well represented in Fig. 6 above PT2. In Fig. 6a, we can observe that the central band at *ca.* 1478 cm^{-1} (the main one at 280–440 K) rapidly gains intensity above PT1 and then starts to disappear above PT2 making its neighbor at 1486 cm^{-1} well noticeable again (below 280 K and above 470 K). This band merging suggests further symmetry increase above PT2, roughly $>470\text{ K}$. In the case of deformation modes, the wavenumbers shift by $1\text{--}2\text{ cm}^{-1}$ in PT1 and up to 4 cm^{-1} in PT2, while their FWHMs increase up to $3/13\text{ cm}^{-1}$ in PT1/PT2 during heating, respectively. This is similar to the changes observed in other crystals containing amines, such as formamidine²⁷ or (multiple)methylammonium.²⁸ The band splitting during the temperature decrease imposed by the symmetry change is best observed for deformations ωCH_2 during the PT2 transition (Fig. S10a, ESI[†]). The skeleton vibrations presented here as νCC modes in Fig. S9b (ESI[†]) are of particular interest as they show greater changes than the methyl(ene) groups. Their wavenumber shifts by $3/7\text{ cm}^{-1}$ and FWHM – by $1/15\text{ cm}^{-1}$ (PT1/PT2). This indicates that the motion of TePrA^+ ions is not only bound to the rearrangement of protons in the molecules but also to the rotation of the skeleton itself. Taking these facts into account together with the thermal behavior of translations and librations of these cations shown in Fig. 6b and Fig. S10d (ESI[†]), one can conclude that PT1 is driven equally by the motions of the TePrA^+ and ClO_4^- ions, while in PT2 the motions of the organic cations have bigger impact compared to the inorganic anions. The observations are consistent with DSC conclusions that PT2 bears resemblance to the phase changes found in liquid crystals when going from crystal at RT to isotropic liquid since the band broadening suggests a melt-like phase.

Dielectric properties

The complex impedance spectroscopy measurements were performed to investigate temperature-variable changes in dielectric function. The frequency dependence on the real (ϵ') and imaginary (ϵ'') parts of complex dielectric permittivity is shown in Fig. 7.

The behavior of the dielectric function (Fig. 7a) exhibits a gradual decline with increasing frequency, while at high frequencies, it remains almost constant and increases with increasing temperature at a given frequency. This dielectric dispersion can be explained by polarization processes. As the frequency increases, the ions cannot follow the applied field, and as a result, a rapid polarization occurs. A high value of the dielectric permittivity at low frequency can be contributed to the presence of space charge polarization, which generates a potential barrier, and results in polarization of bound charge, which leads to higher values of the real part of permittivity.^{30,31} The frequency dependence of the imaginary part of complex permittivity ϵ'' at different temperatures is shown in Fig. 7b. The curve shows almost linear behavior at all temperatures over the entire frequency spectra, which makes an evidence of Ohmic behavior in dielectrics.

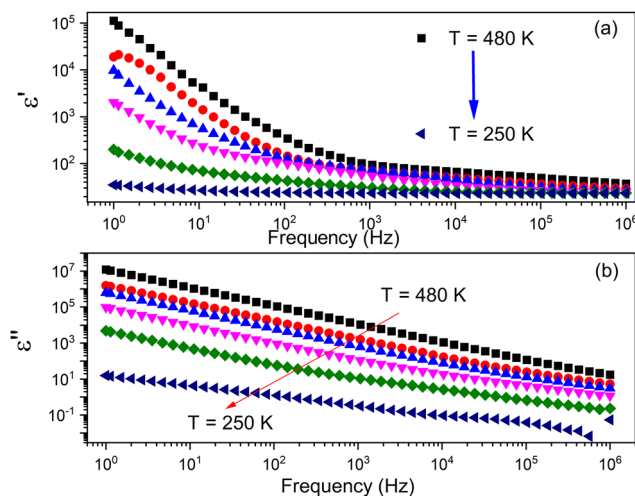


Fig. 7 The frequency dependence on (a) real and (b) imaginary parts of complex permittivity of the TePrAClO_4 compound.

The variation of the real part (ϵ') of the dielectric permittivity as a function of temperature at various frequencies performed on a pressed pellet of TePrAClO_4 is shown in Fig. 8. At low temperatures, a step-like anomaly at around $T_1 = 284\text{ K}$ has been found during the heating and cooling process, whose behavior indicates a structural phase transition. The dielectric permittivity remains almost stable below T_1 , in the LT phase, proving an ordered phase, corresponding to its low-dielectric state. Above 320 K , at RT, ϵ' increases along with temperature, indicating a disturbance of thermal fluctuation and polarization. The order of the ϵ' value in the LT and HT phases is comparable to the nonpolar analogues that show also slight dielectric changes.³ In addition, to investigate the stability in high- and low-dielectric states, the cycles of reversible dielectric switches have been performed (see Fig. 8b).^{32,33} It is shown that with a periodic variation of temperature and the passage of time, the value of the dielectric constant during the transition

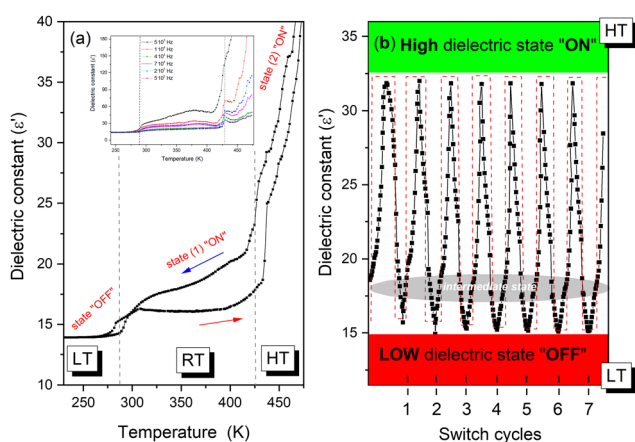


Fig. 8 (a) The temperature-dependence of the real part (ϵ') of the polycrystalline sample at 1 MHz . The inset shows the real part (ϵ') at selected frequencies. (b) The recoverable switching of the dielectric constant between LT and HT phases for 1 MHz .



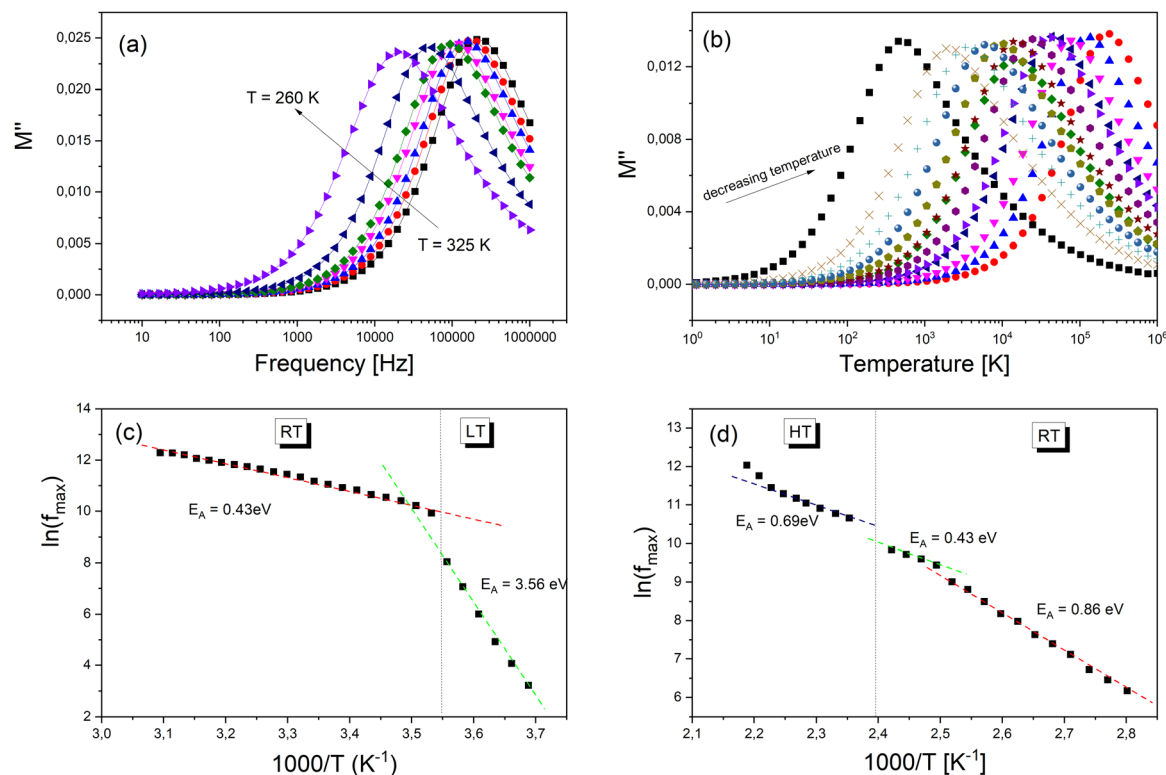


Fig. 9 (a) The frequency dependencies of M'' at different temperatures. (b) The temperature-dependence of M'' at a selected frequency. The variation of relaxation frequency (f_{\max}) with inverse temperature ($1/T$) (c) for PT1 and (d) PT2.

from the HT to LT state remains stable with no decay after several cycles. What is more, during the comparison of the initial dielectric signal between LT and HT phases, no observable weakening during the heating-cooling cycles is reported. This behavior points to switching properties with nearly zero time delay^{32,33} and some potential applications may arise as time-stable and temperature-sensitive devices.

To investigate the electrical response of the material and relaxation processes of materials, the complex modulus $M^*(\omega)$ formalism has been analyzed.³⁴ The complex electric modulus was calculated from the complex electric permittivity given by the following relation:

$$M^*(\omega) = M' + jM'' = \frac{\epsilon'}{\epsilon'^2 - \epsilon''^2} - j \frac{\epsilon''}{\epsilon'^2 - \epsilon''^2}$$

where M' and M'' are the real and imaginary parts of the modulus, respectively.

The evaluation of the imaginary part (M'') of electric modulus as a function of the temperature around PT1 and PT2 transitions is shown in Fig. 9a and b. It is clearly seen that in both cases M'' exhibits a single relaxation peak shifted to a higher frequency with increasing temperature. This proves that the observed relaxations are temperature-dependent. The variation of the relaxation frequency, which corresponds to the frequency at which the M'' peak is well defined, is presented in Fig. 9a and b. The observed relation of $f_{\max}(1/T)$ shows a linear behavior and fulfills the Arrhenius law $f_{\max} = f_0 e^{-E_A/kt}$, where f_0 is the characteristic phonon frequency, E_A is the

activation energy for relaxation, and k is Boltzmann's constant. Using the best least-square fits, the changes in activation energy of dielectric processes resulting from temperature changes have been exposed (Fig. 9c and d). The PTs apparent in the Raman spectroscopy as well in the DSC scans are confirmed by the change of the curve slope at f_{\max} . The observed relaxation process in Fig. 9c with visible changes of its activation energy after PT1 most probably corresponds to an ordering of molecular moieties, like TePrA^+ below 284 K.

Moreover, the variation in the activation energy values in the temperature range between 357 and 476 K visible in Fig. 9d can be explained by the movement in both the cationic and anionic parts. This huge mobility of structure elements in the HT phase is in agreement with the specific data heat and structural results. At the same time, the HT phase is stable up to 520 K which is confirmed by thermogravimetric analysis (Fig. S11, ESI†).

Conclusions

The crystals of the TePrAClO_4 compound undergo two reversible phase transitions at *ca.* $T_1 = 284$ K and at *ca.* $T_2 = 445$ K with extraordinarily large heat and entropy changes for the latter one. The observed phase transition, dielectric and relaxation effects are due to the dynamic motions of the organic cations and anionic framework. Notably, the dielectric function values can be switched and tuned in the low- and high-dielectric

states, which may indicate the potential application of this material in sensors or actuators.

By means of single-crystal XRD, we have been able to structurally characterize the disordered *Pnam* RT phase of TePrAClO₄. The propyl chains of the organic part as well as perchlorate ions are disordered over the mirror plane at $c = 1/4$ and $3/4$. The diffraction measurement confirmed that below PT1, the crystal becomes ordered and its structure is described by the $P2_12_12_1$ space group, LT phase. To verify the structural changes taking place above PT2, the PXRD experiments were performed. The observed reduction in the number of diffraction peaks above PT2 indicates that the HT structure has higher symmetry. The reason for such a change can be found in the increasing level of disorder inherent to the HT phase with entropy change reaching a quite extreme $130 \text{ J mol}^{-1} \text{ K}^{-1}$.

The IR and Raman spectroscopies have proven the order-disorder phase transitions observed using other methods. The main findings are as follows: (i) the persistent absence of the center of symmetry has been deduced from the breaking of the mutual-exclusion rule, (ii) weak intermolecular interactions based on a lesser number of A₁ bands than calculated for a perfect factor-group splitting, (iii) comparable changes in the wavenumber and FWHM shifts in the case of TePrA⁺ and ClO₄[−] ions in PT1 and slightly more significant changes for TePrA⁺ cations (juxtaposed with ClO₄[−] ions) in PT2 lead to the conclusion that PT1 is equally driven by motions of the two ions, while PT2 is more influenced by the motions of organic cations. The most remarkable changes occur in the range of hindered rotations of both ions proving a high degree of disorder and higher symmetry above PT2. It is suggested that PT2 bears a resemblance to the phase change found in liquid crystals when transforming from the crystal at RT to an isotropic liquid.

Conflicts of interest

There are no conflicts to declare.

References

- G. A. Williams, Crystal Structure of Tetraethylammonium Bromopentacarbonyltungstate(0), *Aust. J. Chem.*, 1995, **48**, 1045–1048.
- J. Kivikoski, J. A. K. Howard, P. Kelly and D. Parker, Tetraethylammonium Perchlorate at 150 K, *Acta Crystallogr., Sect. C: Cryst. Struct. Commun.*, 1995, **51**, 535–536.
- H. Y. Ye, J. Z. Ge, Y. Y. Tang, P. F. Li, Y. Zhang, Y. M. You and R. G. Xiong, Molecular Ferroelectric with Most Equivalent Polarization Directions Induced by the Plastic Phase Transition, *J. Am. Chem. Soc.*, 2016, **138**, 13175–13178.
- M. Szafranski, Simple guanidinium salts revisited: Room-temperature ferroelectricity in hydrogen-bonded supramolecular structures, *J. Phys. Chem. B*, 2011, **115**, 8755–8762.
- Q. Pan, Z. B. Liu, H. Y. Zhang, W. Y. Zhang, Y. Y. Tang, Y. M. You, P. F. Li, W. Q. Liao, P. P. Shi, R. W. Ma, R. Y. Wei and R. G. Xiong, A Molecular Polycrystalline Ferroelectric with Record-High Phase Transition Temperature, *Adv. Mater.*, 2017, **29**, 1–7.
- Y. L. Sun, C. Shi and W. Zhang, Distinct room-temperature dielectric transition in a perchlorate-based organic-inorganic hybrid perovskite, *Dalton. Trans.*, 2017, **46**, 16774–16778.
- P. P. Shi, Q. Ye, Q. Li, H. T. Wang, D. W. Fu, Y. Zhang and R. G. Xiong, Crystal structures, phase transitions, and switchable dielectric behaviors: Comparison of a series of N-heterocyclic ammonium perchlorates, *Dalton. Trans.*, 2015, **44**, 8221–8231.
- Y. L. Sun, X. Bin Han and W. Zhang, Structural Phase Transitions and Dielectric Switching in a Series of Organic-Inorganic Hybrid Perovskites ABX₃ (X = ClO₄[−] or BF₄[−]), *Chem. – Eur. J.*, 2017, **23**, 11126–11132.
- Y. Zhang, Y. Liu, H. Y. Ye, D. W. Fu, W. Gao, H. Ma, Z. Liu, Y. Liu, W. Zhang, J. Li, G. L. Yuan and R. G. Xiong, A molecular ferroelectric thin film of imidazolium perchlorate that shows superior electromechanical coupling, *Angew. Chem., Int. Ed.*, 2014, **53**, 5064–5068.
- L. W. Martin and A. M. Rappe, Thin-film ferroelectric materials and their applications, *Nat. Rev. Mater.*, 2016, **2**, 16087.
- T. Fujihara, M. Kato and A. Nagasawa, Tetra-n-propylammonium perchlorate, *Acta Crystallogr., Sect. E: Struct. Rep. Online*, 2005, **61**, 1439–1440.
- CrysAlis PRO, Rigaku Oxford Diffraction, 2018.
- CrysAlis RED, Rigaku Oxford Diffraction, 2019.
- G. M. Sheldrick, Crystal structure refinement with SHELXL, *Acta Crystallogr., Sect. C: Struct. Chem*, 2015, **71**, 3–8.
- O. V. Dolomanov, L. J. Bourhis, R. J. Gildea, J. A. K. Howard and H. Puschmann, OLEX2: A complete structure solution, refinement and analysis program, *J. Appl. Crystallogr.*, 2009, **42**, 339–341.
- K. Brandenburg and M. Berndt, Diamond, Crystal Impact GbR, Bonn, Germany, 1997.
- H. Ono, S. Ishimaru, R. Ikeda and H. Ishida, *Bull. Chem. Soc. Jpn.*, 1997, **70**, 2963–2972.
- W. E. Acree and J. S. Chickos, Phase change enthalpies and entropies of liquid crystals, *J. Phys. Chem. Ref. Data*, 2006, **35**, 1051–1330.
- Y. Ogawa and K. Ootani, Phase transitions of dimeric liquid crystals containing long odd-numbered methylene spacers, *Polym. J.*, 1999, **31**, 51–54.
- T. Ying, Y. Huang, N. Song, Y. Tan, Y. Tang, Z. Sun, J. Zhuang and X. Dong, Dielectric switching from a high temperature plastic phase transition in two organic salts with chiral features, *Mater. Adv.*, 2022, **3**, 1581–1586.
- M. Trzebiatowska-Gusowska and A. Gągor, The order-disorder state of diaminoalkanes in Cu-based metal-organic materials, *J. Coord. Chem.*, 2017, **70**, 1536–1547.
- J. G. Contreras, C. A. López and G. V. Seguel, “Vibrational Spectra of Tetrapropylammonium Trichlorozincate(II)”, *Spectrosc. Lett.*, 1985, **18**, 71–78.
- E. Szostak and A. Migdał-Mikuli, Thermal analysis, phase transitions and molecular reorientations in [Fe(OS(CH₃)₂)₆](ClO₄)₂, *J. Therm. Anal. Calorim.*, 2017, **129**, 1151–1158.
- D. L. Lewis, E. D. Estes and D. J. Hodgson, The infrared spectra of coordinated perchlorates, *J. Cryst. Mol. Struct.*, 1975, **5**, 67–74.



- 25 B. B. Holló, V. M. Petruševski, G. B. Kovács, F. P. Franguelli, A. Farkas, A. Menyhárd, G. Lendvay, I. E. Sajó, L. Nagy-Bereczki, R. P. Pawar, I. M. Szilágyi, E. Bódis and L. Kótai, Thermal and spectroscopic studies on a double-salt-type pyridine-silver perchlorate complex having $\kappa 1$ -O coordinated perchlorate ions, *J. Therm. Anal. Calorim.*, 2019, **138**, 1193–1205.
- 26 A. R. Aliev, I. R. Akhmedov, M. G. Kakagasanov and Z. A. Aliev, Pre-Transition Phenomena in the Temperature Range of Structural Phase Transitions in Perchlorate Crystals, *Russ. J. Phys. Chem. A*, 2020, **94**, 1363–1368.
- 27 M. Trzebiatowska, A. Gągor, L. Macalik, P. Peksa and A. Sieradzki, Phase transition in the extreme: a cubic-to-triclinic symmetry change in dielectrically switchable cyanide perovskites, *Dalton. Trans.*, 2019, **48**, 15830–15840.
- 28 M. Trzebiatowska, The spectroscopic study of phase transitions in the series of cyanide perovskites, *Spectrochim. Acta, Part A*, 2021, **245**, 118957.
- 29 Y. Chen, Y. H. Zhang and L. J. Zhao, ATR-FTIR spectroscopic studies on aqueous LiClO_4 , NaClO_4 , and $\text{Mg}(\text{ClO}_4)_2$ solutions, *Phys. Chem. Chem. Phys.*, 2004, 537–542.
- 30 M. Abdullah Dar, K. Majid, K. M. Batoo and R. K. Kotnala, Dielectric and impedance study of polycrystalline $\text{Li}_{0.35-0.5}\text{XCd}_{0.3}\text{NiXFe}_{2.35-0.5}\text{XO}_4$ ferrites synthesized via a citrate-gel auto combustion method, *J. Alloys Compd.*, 2015, **632**, 307–320.
- 31 C. G. Koops, On the dispersion of resistivity and dielectric constant of some semiconductors at audiofrequencies, *Phys. Rev.*, 1951, **83**, 121–124.
- 32 K. Pasińska, A. Ciupa, A. Pikul, A. Gągor, A. Pietraszko and A. Ciżman, 1D metal-oxalates $\text{H}_2\text{DABCO}[\text{M}(\text{C}_2\text{O}_4)_2]\cdot 3\text{H}_2\text{O}$ (M(ii): Co, Mg, Zn): Phase transitions and magnetic, dielectric, and phonon properties, *J. Mater. Chem. C*, 2020, **8**, 6254–6263.
- 33 A. Cizman, D. Kowalska, M. Trzebiatowska, W. Medycki, M. Krupiński, P. Staniorowski and R. Poprawski, The structure and switchable dielectric properties of a dabco complex with chromium chloride, *Dalton. Trans.*, 2020, **49**, 10394–10401.
- 34 M. Kaiser, Magnetic and electric modulus properties of in substituted Mg-Mn-Cu ferrites, *Mater. Res. Bull.*, 2016, **73**, 452–458.

